

Thermodynamic Analysis Using First-Principles Calculations of Phases and Structures of $\text{Li}_x\text{Ni}_{0.5}\text{Mn}_{1.5}\text{O}_4$ ($0 \leq x \leq 1$)

Ippei Kishida,* Kengo Orita, Atsutomo Nakamura, and Yoshiyuki Yokogawa

Department of Mechanical Engineering,

Faculty of Engineering, Osaka City University,

3-3-138 Sugimoto, Sumiyoshi-ku, Osaka 558-8585, Japan

(Dated: March 7, 2018)

Abstract

$\text{LiNi}_{0.5}\text{Mn}_{1.5}\text{O}_4$, which has a spinel framework structure, is a promising candidate for the cathode material of next-generation lithium-ion batteries with high energy density. We investigate the structural transition in $\text{Li}_x\text{Ni}_{0.5}\text{Mn}_{1.5}\text{O}_4$ ($0 \leq x \leq 1$) through first-principles calculations using the projector augmented wave method with the generalized gradient approximation. We calculate all the unique Li-site occupation configurations in a unit cell to obtain the total energies and the most stable structures for various compositions. Thermodynamic analysis shows that $\text{Li}_{0.5}\text{Ni}_{0.5}\text{Mn}_{1.5}\text{O}_4$ with $x = 0.5$ is the only stable phase for $0 < x < 1$. The decomposition energy is lower than 0.1 eV for $0 < x < 0.5$, but is distinctly higher for $0.5 < x < 1$. The decomposition energy reaches 0.39 eV at $x = 0.75$. The ratios of the structures at room temperature are calculated from Boltzmann factors by using the energy differences between structures. The crystal structure of the unit cell changes gradually from $x = 0$ to 0.5, but changes markedly from $x = 0.5$ to 1. This first-principles study provides a general evaluation of the variation in the crystal structure with the composition of the bulk material, which affects the cyclability of the electrode.

PACS numbers: 61.50.Ah, 64.60.-i, 64.70.qd, 71.15.Nc

Keywords: ab initio calculation, thermodynamic stability, crystal structure, electrochemical potential,

I. INTRODUCTION

the high energy density of lithium-ion batteries makes them particularly suitable energy storage devices for the many new portable electronic devices that are coming onto the market. LiCoO_2 is widely used as a cathode material for lithium-ion batteries, because it has a voltage of up to 4 V versus metallic lithium¹. Voltage is a fundamental property of batteries; higher voltages are closely related to larger electrical energy capacities and faster electronic performance in processing units. Recently, several transition-metal-doped spinel cathode materials with voltages of 5 V, such as $\text{LiM}_x\text{Mn}_{2-x}\text{O}_4$ ($M = \text{Ni, Cr, Co, Fe, Cu}$), have been reported²⁻⁵. $\text{LiNi}_{0.5}\text{Mn}_{1.5}\text{O}_4$ is a particularly promising material because of its high voltage, electrochemical stability, and lack of trace metal impurities^{6,7}. Furthermore, materials such as $\text{Li}[\text{MnNiCo}]\text{O}_2$ ^{5,8}, $\text{Li}[\text{MnNiCr}]\text{O}_2$ ⁹, and $\text{Li}[\text{MnNiFeCo}]\text{O}_2$ ¹⁰ are based on $\text{LiNi}_{0.5}\text{Mn}_{1.5}\text{O}_4$. The physical and chemical properties of $\text{LiNi}_{0.5}\text{Mn}_{1.5}\text{O}_4$ have been experimentally determined by X-ray diffraction, scanning electron microscopy, infrared-Raman spectroscopy, electron diffraction, and cyclic voltammetry¹¹⁻¹³. Although the crystallographic and electrochemical properties of $\text{LiNi}_{0.5}\text{Mn}_{1.5}\text{O}_4$ have been well reported, the microscopic changes in the crystal structure and electrochemical properties during the lithiation and delithiation of an $\text{Li}_x\text{Ni}_{0.5}\text{Mn}_{1.5}\text{O}_4$ crystal are not yet fully understood. Charging and discharging are primary functions of secondary batteries; therefore, the change in the composition and structure of electrodes is unavoidable, and the changes influence cyclability. Predicting these structural changes will help to accelerate the development of electrode materials.

Theoretical and microstructural analysis can provide a valuable alternative to experimental studies for understanding the properties of materials. First-principles calculation based on density functional theory (DFT) is among the most powerful methods for determining the fundamental characteristics of electrodes. The theoretical band structures and crystal structures of various Li-transition metal oxides, including LiMnO_2 ^{14,15} and LiMn_2O_4 ¹⁶, have been thoroughly investigated. Several studies using theoretical calculations and basic thermodynamic models have shown that the average electrochemical potential of $\text{LiNi}_{0.5}\text{Mn}_{1.5}\text{O}_4$ is derived from the difference in total energy between the fully lithiated and delithiated materials^{14,17,18}. However, a method has not yet been established for evaluating the changes in crystal structure and electrochemical potential with varying Li composition. To analyze the properties of crystals at intermediate compositions quantitatively, we investigated the

sublattice structures of Li and used DFT to evaluate their thermodynamic stability at various compositions between $\text{Ni}_{0.5}\text{Mn}_{1.5}\text{O}_4$ and $\text{LiNi}_{0.5}\text{Mn}_{1.5}\text{O}_4$. We propose a method for predicting the average electrochemical potential as well as the change in electrochemical potential as the composition of the bulk material is varied. This information is useful for designing new electrode materials, because the electrochemical potential and cyclability of an electrode material is strongly affected by the change in the atomic structure during lithiation and delithiation.

II. COMPUTATIONAL PROCEDURE

A. Crystal Structure

The starting structure for our study was a unit cell of $\text{LiNi}_{0.5}\text{Mn}_{1.5}\text{O}_4$ crystal (Fig. 1). The cell belongs to the $P4_332$ space group and consists of 8 formula units containing 56 atoms in total: $\text{Li}_8\text{Ni}_4\text{Mn}_{12}\text{O}_{32}$ ¹¹. The O atoms are located at the 8(c) and 24(e) sites, and form a distorted face-centered cubic (fcc) structure in the cell. Cations occupy the ordered polyhedral sites formed by the O sublattice; the Li, Ni, and Mn atoms are present in the octahedral 8(c) sites, 4(b) sites, and 12(d) sites, respectively. The Li sublattice forms a slightly distorted diamond structure. The eight Li sites in the unit cell were labeled as shown in Table I. The initial cells for geometry optimization at various compositions were made by removing n ($n = 0, 1, 2, \dots, 8$) Li atoms from the $\text{Li}_8\text{Ni}_4\text{Mn}_{12}\text{O}_{32}$ cell, resulting in a $\text{Li}_{8-n}\text{Ni}_4\text{Mn}_{12}\text{O}_{32}$ cell. The Li sites are symmetrically equivalent in the space group. Therefore, for $n = 0, 1, 7$, and 8 , the unit cell crystal structure is the same. For $2 \leq n \leq 6$, the configurations of the occupied and unoccupied Li sites were considered. We calculated all the unique configurations in the symmetry operations of its space group (Table II). The geometry of each cell was optimized to obtain the most stable lattice volume, shape, and atomic coordinates; the total energies of the cells were computed at the same time. We examined differences in energy of the various structures. The change in Gibbs energy is expressed by $\Delta G = \Delta E + P\Delta V - T\Delta S$. However, ΔE was of the order of 0.04-4 (eV/cell), $P\Delta V$ was of the order of 10^{-5} (eV/cell), and $T\Delta S$ was of the order of the thermal energy in this study^{14,19,20}. Because the $P\Delta V$ and $T\Delta S$ terms have little effect on ΔG , the assumption that ΔG can be approximated by only the change in the internal energy, ΔE , is valid.

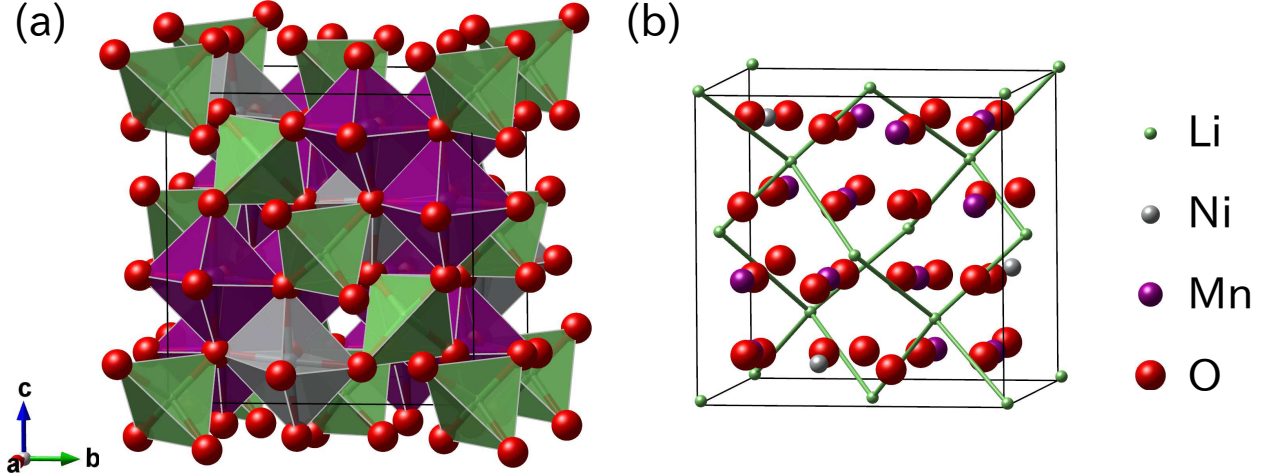


FIG. 1. (Color online) Crystal structure of $\text{LiNi}_{0.5}\text{Mn}_{1.5}\text{O}_4$. The Li, Ni, Mn, and O ions are shown in green, gray, purple, and red, respectively. The radii are different to allow them to be clearly distinguished: $r_{\text{Li}} < r_{\text{Ni}} < r_{\text{Mn}} < r_{\text{O}}$. (a) O polyhedra including cations. The tetrahedra (green), light gray octahedra, and dark gray octahedra (purple) indicate the LiO_4 , NiO_6 , and MnO_6 polyhedra, respectively. (b) Li-Li bonding in the Li sublattice.

TABLE I. Labels and internal coordinates of Li sites in the unit cell. These coordinates are adjusted to those of the ideal diamond structure to allow for easy recognition.

axis	L000	L220	L111	L331	L202	L022	L313	L133
a	0	0.5	0.25	0.75	0.5	0	0.75	0.25
b	0	0.5	0.25	0.75	0	0.5	0.25	0.75
c	0	0	0.25	0.25	0.5	0.5	0.75	0.75

B. Thermodynamic analysis of phases

The ratio of structures at equilibrium was determined for a total Li content in the bulk of $x = b$. The lithiated and delithiated material was assumed to be $\text{Li}_x X$, where X was $\text{Ni}_{0.5}\text{Mn}_{1.5}\text{O}_4$. Because this is a pseudo-unitary system of Li, we examine Li content only. For compositions of $x = a, b$, and c ($a < b < c$) in $\text{Li}_x X$, the decomposition reaction is

$$\text{Li}_b X \rightarrow \frac{c-b}{c-a} \text{Li}_a X + \frac{b-a}{c-a} \text{Li}_c X. \quad (1)$$

TABLE II. Unique configurations of occupied and unoccupied Li sites in a unit cell of $\text{Li}_n\text{Ni}_4\text{Mn}_{12}\text{O}_{32}$. All configurations are assigned an uppercase character from A to W. The filled circles and dashes indicate occupied and unoccupied sites, respectively. The labels at the top, for example L000, are site names, which are the same as those in Table I.

n	structure	L000	L220	L111	L331	L202	L022	L313	L133
0	A	-	-	-	-	-	-	-	-
1	B	•	-	-	-	-	-	-	-
2	C	•	•	-	-	-	-	-	-
2	D	•	-	•	-	-	-	-	-
2	E	•	-	-	•	-	-	-	-
3	F	•	•	•	-	-	-	-	-
3	G	•	•	-	•	-	-	-	-
3	H	•	•	-	-	•	-	-	-
4	I	•	•	•	•	-	-	-	-
4	J	•	•	•	-	•	-	-	-
4	K	•	•	•	-	-	-	•	-
4	L	•	•	•	-	-	-	-	•
4	M	•	•	-	•	•	-	-	-
4	N	•	•	-	•	-	-	-	•
4	O	•	•	-	-	•	•	-	-
5	P	•	•	•	•	•	-	-	-
5	Q	•	•	•	•	-	•	-	-
5	R	•	•	•	-	•	•	-	-
6	S	•	•	•	•	•	•	-	-
6	T	•	•	•	•	•	-	•	-
6	U	•	•	•	•	-	•	•	-
7	V	•	•	•	•	•	•	•	-
8	W	•	•	•	•	•	•	•	•

The decomposition energy of this reaction, $\Delta G_b(a, c)$, is

$$\Delta G_b(a, c) = G(b) - \left(\frac{c-b}{c-a} G(a) + \frac{b-a}{c-a} G(c) \right),$$

where $G(x)$ is the Gibbs energy of the most stable structure at composition x . Positive values of $\Delta G_b(a, c)$ indicate that the left side of Eq. (1) is thermodynamically unstable, whereas negative values indicate that it is stable. $\Delta G_b(a, c)$ gives the ratio of the equilibrium amounts of species on each side of Eq. (1) by using the Boltzmann factor,

$$\frac{P_b(a, c)}{P_b(b)} = \exp\left(\frac{\Delta G_b(a, c)}{kT}\right), \quad (2)$$

where $P_b(b)$ and $P_b(a, c)$ are the ratios of both edges in Eq. (1) in the bulk, k is the Boltzmann constant, and T is the temperature. T was assumed to be room temperature, 298 K. The sum of the ratios of all states at a given a given value of b must be 1:

$$P_b(b) + \sum_{0 \leq a < b} \sum_{b < c \leq 1} (P_b(a, c)) = 1. \quad (3)$$

The composition was treated as a discrete value. Each ratio of the decomposed state in the bulk, $P_b(a, c)$ and $P_b(b)$, was calculated by solving simultaneous equations 2 and 3. Then, each ratio, $P_b(x)$, was derived from

$$P_b(x) = \begin{cases} \sum_{b < c \leq 1} \frac{c-b}{c-x} P_b(x, c) & (x < b) \\ P_b(b) & (x = b) \\ \sum_{0 \leq a < b} \frac{b-a}{x-a} P_b(a, x) & (x > b). \end{cases} \quad (4)$$

Assuming that ideal monovalent Li^+ cations are the only charge carriers, the average electrochemical potential versus Li/Li^+ between $x_1 < x < x_2$ of $\text{Li}_x X$, $V(x)$, is given by

$$V(x) = -\frac{1}{F} \left(\frac{G(x_2) - G(x_1)}{x_2 - x_1} - G_{\text{Li}} \right), \quad (5)$$

where F is the Faraday constant, and G_{Li} is the chemical potential of Li in a metallic Li anode^{14,19,21}.

C. Computational conditions

The spin-polarized calculations were performed by DFT^{22,23} using the plane-wave projector augmented-wave method²⁴ as implemented in the VASP code.²⁵⁻²⁷ The exchange-correlation term was treated with the Perdew-Burke-Ernzerhof functional²⁸. For the unit

cell of $\text{Li}_x\text{Ni}_{0.5}\text{Mn}_{1.5}\text{O}_4$, a cutoff energy of 500 eV and a k -mesh of $4 \times 4 \times 4$ were determined through preliminary test calculations. A cutoff energy of 500 eV and a k -mesh of $64 \times 64 \times 64$ were calculated for Li metal in a primitive cell with body-centered cubic structure. Geometry optimization was truncated when the residual forces on the atoms became less than 0.02 eV/Å.

III. RESULTS AND DISCUSSION

A. Thermodynamic stability and phase transition

Fig. 2 shows the calculated energies of all the structures after geometry optimization. For clarity, the values of energies shown on the vertical axis, $G'(x)$, were corrected with linearly approximated chemical potential of Li, μ'_{Li} :

$$\mu'_{\text{Li}} = G(1) - G(0) \quad (6)$$

$$G'(x) = G(x) - (G(0) + x\mu'_{\text{Li}}). \quad (7)$$

The line connecting the energies of the most stable structures for neighboring compositions was concave except for the area around $x = 0.5$ (Fig. 2). This indicates that only one composition, $x = 0.5$, was thermodynamically stable, except for the end member compositions, $x = 0$ and 1. The Li sublattice in the cell labeled O forms an fcc-like structure. The fcc structure has high symmetry and uniform distance between atoms. The electrostatic repulsion between Li^+ ions makes it preferable for them to be positioned as far apart as possible. Thus, the high stability of the cell is reasonable. In the region $0 < x < 0.5$, the energy profile was concave, suggesting that $\text{Li}_x\text{Ni}_{0.5}\text{Mn}_{1.5}\text{O}_4$ should decompose to $\text{Ni}_{0.5}\text{Mn}_{1.5}\text{O}_4$ and $\text{Li}_{0.5}\text{Ni}_{0.5}\text{Mn}_{1.5}\text{O}_4$ at 0 K. However, the decomposition energy, $\Delta E_x(0, 0.5)$, was less than 0.1 eV. This slight instability would produce the structures labeled B, C, and H at intermediate compositions through the thermal effect, even at room temperature. The most stable structure changes were A, B, C, H, and O for compositions varying from $x = 0$ to $x = 0.5$. Table II shows that the change in the most stable structure between neighboring compositions can be represented by replacing occupied Li sites with unoccupied sites, or unoccupied sites with occupied sites. For example, the only difference between structures H and O is at the L022 site. This simple mechanism would result in smooth changes in the atomic structure as the composition changes and may contribute to good cyclability. In contrast,

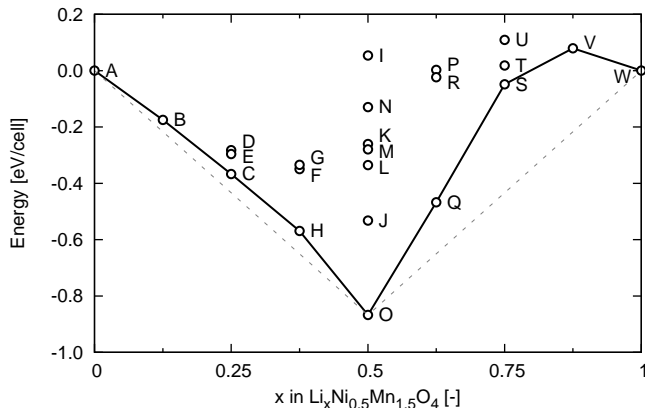


FIG. 2. Energies of crystal structures with a composition of $\text{Li}_x\text{Ni}_{0.5}\text{Mn}_{1.5}\text{O}_4$. Each energy on the vertical axis is corrected by linear approximation of the Li chemical potential (Eqs. 6 and 7). Labels A to W correspond to those in Table II. The solid line connects the most stable structures at the various compositions. The dotted line connects all the thermodynamically stable structures between $\text{Ni}_{0.5}\text{Mn}_{1.5}\text{O}_4$ and $\text{LiNi}_{0.5}\text{Mn}_{1.5}\text{O}_4$.

the decomposition energy, $\Delta E_x(0.5, 1)$, was high in the region $0.5 < x \leq 1$. In particular, $\Delta E_{0.75}(0.5, 1)$ was 0.39 eV for structure S. The bulk material should be a mixture of two separate phases, namely, structures O and W. Therefore, the crystal structure of the unit cell changed considerably in this region. The cells that transformed from $\text{Li}_{0.5}\text{Ni}_{0.5}\text{Mn}_{1.5}\text{O}_4$ to $\text{LiNi}_{0.5}\text{Mn}_{1.5}\text{O}_4$ were stressed by the volume change, which was estimated to be about 4%.

The most stable structures, which are on the solid line in Fig. 2, are dominant at certain concentrations because of the Boltzmann factor. Therefore, we can assume that they are the only structures in the bulk material. We used the energies in Fig. 2 and Eq. 4 to calculate the ratio of structures in bulk $\text{Li}_x\text{Ni}_{0.5}\text{Mn}_{1.5}\text{O}_4$ at 298 K (Fig. 3). This figure shows that the unit cell structure changed gradually via intermediate concentrations when the total Li content x was varied from 0 to 0.5, whereas the structure changed markedly from $x = 0.5$ to 1. These results suggest that it would be difficult to detect a difference in the internal structure of $\text{Li}_x\text{Ni}_{0.5}\text{Mn}_{1.5}\text{O}_4$ ($0 \leq x \leq 0.5$) by experimental methods. The cyclability of an electrode is expected to depend on how smoothly its crystal structure changes. Therefore, it is valuable to describe the change in structure quantitatively as in Fig. 3 in order to predict

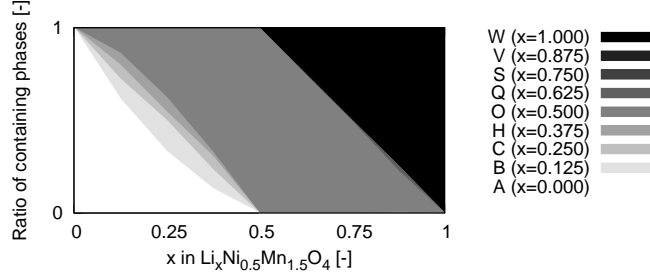


FIG. 3. Calculated ratio of structures in bulk $\text{Li}_x\text{Ni}_{0.5}\text{Mn}_{1.5}\text{O}_4$ at 298 K. The value of x on the horizontal axis indicates the total Li content in the bulk. Darker areas indicate structures with higher Li concentration. The uppercase characters in the legend indicate structures corresponding to those in Table II and Fig. 2. The value of x for each of the uppercase characters indicates the Li occupancy of the structures.

the durability of new electrode materials.

B. Electrochemical potential

There were three thermodynamically stable compositions, where $x = 0, 0.5,$ and 1 . The electrochemical potential in the region $0 < x < 0.5$ and $0.5 < x < 1$ was calculated by using Eq. (5). Fig. 4 shows the variation of the electrochemical potential with the total Li content in a bulk electrode. The calculated values of 3.99 and 3.56 V were lower than the experimental values of 4.739 and 4.718 V¹¹. However, first-principles calculations using the generalized gradient approximation typically give underestimates¹⁴, and the calculated and experimental results showed good agreement. The total change in the theoretical electrochemical potentials for compositions of $0 \leq x \leq 1$ was calculated as 0.43 V. The changes in the electrochemical potential shown in Fig. 4 correspond to the changes in the slope of the dotted line in Fig. 2 because the electrochemical potential is reflected in μ_{Li} of the material. The small change in electrochemical potential resulted from $\text{Li}_{0.5}\text{Ni}_{0.5}\text{Mn}_{1.5}\text{O}_4$ being only slightly stable, that is, having slightly negative decomposition energy. the small stability

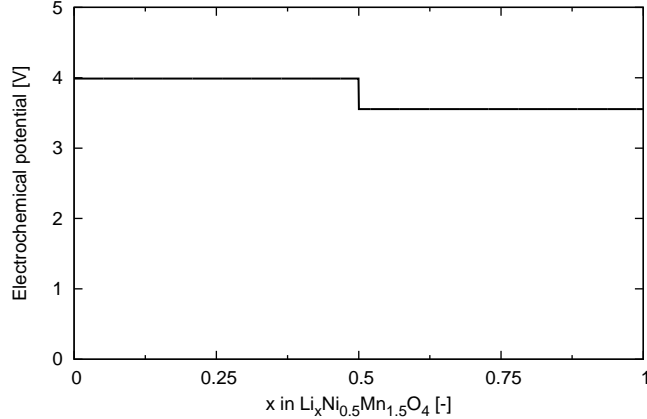


FIG. 4. Calculated changes in the electrochemical potential of $\text{Li}_x\text{Ni}_{0.5}\text{Mn}_{1.5}\text{O}_4$ versus Li/Li^+ .

of $\text{Li}_{0.5}\text{Ni}_{0.5}\text{Mn}_{1.5}\text{O}_4$. If there were no stable phase in intermediate composition of Li_xX , the material would theoretically have constant electrochemical potential. However, during lithiation and delithiation, an intermediate composition that is highly unstable results in a sharp change in atomic structure, which is an obstacle to good cyclability.

IV. CONCLUSION

In summary, first-principles calculations revealed the microscopic structure and stability of $\text{LiNi}_{0.5}\text{Mn}_{1.5}\text{O}_4$, which is among the most promising materials for lithium-ion battery cathodes. We quantitatively evaluated the energies of all the configurations of Li-site occupation for intermediate compositions of $\text{Li}_x\text{Ni}_{0.5}\text{Mn}_{1.5}\text{O}_4$ ($0 \leq x \leq 1$). In this way, we assessed the thermodynamic stability of each structure and the change in the electrochemical potential with varying total Li content in the bulk. $\text{Li}_{0.5}\text{Ni}_{0.5}\text{Mn}_{1.5}\text{O}_4$ ($x = 0.5$) was the only stable phase for $0 < x < 1$. The decomposition energy was lower than 0.1 eV for $0 < x < 0.5$, but was high for $0.5 < x < 1$. The thermodynamic analysis showed that the change in structure with varying Li content was gradual for low Li content compositions, and rapid for high Li content compositions. The theoretical change in electrochemical potential at $x = 0.5$ was found to be 0.43 V, which reflects $\text{Li}_{0.5}\text{Ni}_{0.5}\text{Mn}_{1.5}\text{O}_4$ having lower stability than $\text{Ni}_{0.5}\text{Mn}_{1.5}\text{O}_4$ and $\text{LiNi}_{0.5}\text{Mn}_{1.5}\text{O}_4$. We have demonstrated that theoretical calculations can reveal precise changes in structure, phase, and electrochemical potential and can

explain the cyclability of electrode materials. In particular, visualizing the change in the crystal structure as shown in Fig. 3 will be particularly valuable for discovering durable electrode materials.

ACKNOWLEDGMENTS

We thank Dr. K. Ariyoshi for fruitful discussion.

* kishida@imat.eng.osaka-cu.ac.jp

- ¹ K. Mizushima, P. Jones, P. Wiseman, and J. Goodenough, *Materials Research Bulletin* **15**, 783 (1980).
- ² R. Koksang, J. Barker, H. Shi, and M. Saïdi, *Solid State Ionics* **84**, 1 (1996).
- ³ B. Xu and S. Meng, *Journal of Power Sources* **195**, 4971 (2010).
- ⁴ A. Churikov and V. Sycheva, *Russian Journal of Electrochemistry* **47**, 1117 (2011).
- ⁵ Y. Cho, S. Lee, Y. Lee, T. Hong, and J. Cho, *Advanced Energy Materials* **1**, 821 (2011).
- ⁶ Q. Zhong, *Journal Of The Electrochemical Society* **144**, 205 (1997).
- ⁷ H.-s. Fang, Z.-x. Wang, X.-h. Li, H.-j. Guo, and W.-j. Peng, *Journal of Power Sources* **153**, 174 (2006).
- ⁸ L. Wu, K.-W. Nam, X. Wang, Y. Zhou, J.-C. Zheng, X.-Q. Yang, and Y. Zhu, *Chemistry of Materials* **23**, 3953 (2011).
- ⁹ N. K. Karan, D. P. Abraham, M. Balasubramanian, M. M. Furczon, R. Thomas, and R. S. Katiyar, *Journal of The Electrochemical Society* **156**, A553 (2009).
- ¹⁰ J.-t. Son and E. Cairns, *Korean Journal Of Chemical Engineering* **24**, 888 (2007).
- ¹¹ K. Ariyoshi, Y. Iwakoshi, N. Nakayama, and T. Ohzuku, *Journal of The Electrochemical Society* **151**, A296 (2004).
- ¹² A. Mat, K. S. Sulaiman, and M. A. Sulaiman, *Solid State Science and Technology* **14**, 141 (2006).
- ¹³ H. Xia, S. Tang, L. Lu, Y. Meng, and G. Ceder, *Electrochimica Acta* **52**, 2822 (2007).
- ¹⁴ M. Aydinol, A. Kohan, G. Ceder, K. Cho, and J. Joannopoulos, *Physical Review B* **56**, 1354 (1997).

- ¹⁵ Y. Koyama, I. Tanaka, and H. Adachi, *Advances in Quantum Chemistry* **42**, 145 (2003).
- ¹⁶ Y. Koyama, I. Tanaka, H. Adachi, Y. Uchimoto, and M. Wakihara, *Journal of The Electrochemical Society* **150**, A63 (2003).
- ¹⁷ M. K. Aydinol, A. F. Kohan, and G. Ceder, *Journal of Power Sources* **68**, 664 (1997).
- ¹⁸ T.-F. Yi, Y.-R. Zhu, and R.-S. Zhu, *Solid State Ionics* **179**, 2132 (2008).
- ¹⁹ M. K. Aydinol and G. Ceder, *Journal of the Electrochemical Society* **144**, 3832 (1997).
- ²⁰ I. A. Courtney, J. S. Tse, O. Mao, J. Hafner, and J. R. Dahn, *Physical Review B* **58**, 15583 (1998).
- ²¹ V. Chevrier, S. Ong, R. Armiento, M. Chan, and G. Ceder, *Physical Review B* **82**, 075122 (2010).
- ²² P. Hohenberg and W. Kohn, *Physical Review* **136**, B864 (1964).
- ²³ W. Kohn and L. J. Sham, *Physical Review* **140**, A1133 (1965).
- ²⁴ P. E. Blöchl, *Physical Review B* **50**, 17953 (1994).
- ²⁵ G. Kresse and J. Hafner, *Physical Review B* **47**, 558 (1993).
- ²⁶ G. Kresse and J. Furthmüller, *Physical review B* **54**, 11169 (1996).
- ²⁷ G. Kresse and D. Joubert, *Physical Review B* **59**, 1758 (1999).
- ²⁸ J. P. Perdew, K. Burke, and M. Ernzerhof, *Physical Review Letters* , 3865 (1996).

